Pressure-enthalpy formulation for numerical simulations of supercritical water/steam systems applied to a reservoir in Tuscany, Italy

Henrik Büsing, Jan Niederau, Christoph Clauser

Institute for Applied Geophysics and Geothermal Energy, E.ON Energy Research Center,

RWTH Aachen University, Aachen, Germany

hbuesing@eonerc.rwth-aachen.de

Keywords: pressure-enthalpy formulation, numerical simulation, two-phase water/steam system.

GLOSSARY

ϕ	Porosity
$\rho_{w,n,s}$	Density **w**etting phase, **n**on-wetting phase, **s**olid matrix [kg m^{-3}]
$S_{w,n}$	Saturation **w**etting phase, **n**on-wetting phase, with $S_w + S_n = 1$
t	Time [s]
$k_{r,w,n}$	Relative permeability of **w**etting phase, **n**on-wetting phase
$\boldsymbol{K}$	Permeability tensor [m²]
$p_{w,n}$	Pressure of **w**etting phase, **n**on-wetting phase, with $p_c = p_n - p_w$
g	Gravitational acceleration [m s^{-2}]
q^w	Source term [kg m^{-3} s^{-1}]
$u_{w,n}$	Specific internal energy of **w**etting phase, **n**on-wetting phase [J kg^{-1}]
$h_{w,n}$	Specific enthalpy of the **w**etting phase, **n**on-wetting phase [J kg^{-1}]
c_s	Specific heat capacity of the solid matrix [W kg^{-1} K^{-1}]
λ_{pm}	Tensor of mean thermal conductivity of the filled **p**orous **m**atrix [W m^{-1} K^{-1}]
q^h	Heat generation term [W m^{-3}]

ABSTRACT

We implement a water pressure-enthalpy formulation in our in-house code SHEMAT-Suite. Our formulation consists of a mass balance equation for the two phases, water and steam, complemented by a single energy balance equation, assuming local thermodynamic equilibrium. We verify the implementation by comparison with existing (semi-) analytical and numerical solutions for pressures, temperatures and saturations. Finally, we apply our formulation to a supercritical water/steam reservoir located in Tuscany, Italy. We show numerical simulations of this reservoir including phase changes from water to steam and conditions ranging from liquid/gas to supercritical.

1. INTRODUCTION

Numerical simulations offer the opportunity to gain insight into otherwise not accessible systems. Deep geothermal reservoirs, as all geological reservoirs, can only be characterized through sparse and uncertain data from, e.g., boreholes, outcrops at the surface or geophysical exploration methods. Nevertheless, information on temperature at depth is crucial to assess the productivity of a drilled well. This knowledge can make the difference between a successful drilling and a financial failure.

The results of a numerical simulation depend on the geological model, the equations governing the physical behaviour, and the accuracy of the numerical method employed. Here, we focus on the equations and the numerical method, verifying that we solve the equations correctly. For a discussion of the geological model of the geothermal reservoir in Tuscany, Italy we refer to the European Geothermal Congress extended abstract of Niederau et al. (2016).

This extended abstract is organized as follows: In a first section we describe the mathematical equations we use. Subsequently, we discuss the numerical method employed to solve these equations. In a third section we present several test examples comparing the numerical results with given analytical, semi-analytical and numerical solutions available. Finally,

we present simulation results for the actual geothermal reservoir in Tuscany.

2. Mathematical Model

The equations used consist of a mass balance for the two phases, water and steam, complemented by a single energy balance equation assuming local thermodynamic equilibrium (Faust and Mercer, 1979).

Mass transport is calculated by the following equation (symbols and units explained in the glossary):

$$\phi\frac{\partial(\varrho_{\mathrm{w}}S_{\mathrm{w}})}{\partial t} + \phi\frac{\partial(\varrho_{\mathrm{n}}S_{\mathrm{n}})}{\partial t} - \nabla\cdot\left(\frac{k_{\mathrm{r,w}}}{\mu_{\mathrm{w}}}\varrho_{\mathrm{w}}\mathbf{K}\left(\nabla p_{\mathrm{w}} - \varrho_{\mathrm{w}}\mathbf{g}\right)\right) - \nabla\cdot\left(\frac{k_{\mathrm{r,g}}}{\mu_{\mathrm{n}}}\varrho_{\mathrm{n}}\mathbf{K}\left(\nabla p_{\mathrm{n}} - \varrho_{\mathrm{n}}\mathbf{g}\right)\right) = q^{\mathrm{w}} \quad [1]$$

Two phases are taken into account by considering saturations (S_w, and S_n), as well as relative permeabilities ($k_{r,w}$, and $k_{r,n}$).

Heat transport can be described by the following energy balance equation:

$$\phi\frac{\partial(\varrho_{\mathrm{w}}u_{\mathrm{w}}S_{\mathrm{w}})}{\partial t} + \phi\frac{\partial(\varrho_{\mathrm{n}}u_{\mathrm{n}}S_{\mathrm{n}})}{\partial t} + (1-\phi)\frac{\partial(\varrho_{\mathrm{s}}c_{\mathrm{s}}T)}{\partial t} - \nabla\cdot\left(\frac{k_{\mathrm{r,w}}}{\mu_{\mathrm{w}}}\varrho_{\mathrm{w}}h_{\mathrm{w}}\mathbf{K}\left(\nabla p_{\mathrm{w}} - \varrho_{\mathrm{w}}\mathbf{g}\right)\right) - \nabla\cdot\left(\frac{k_{\mathrm{r,g}}}{\mu_{\mathrm{n}}}\varrho_{\mathrm{n}}h_{\mathrm{n}}\mathbf{K}\left(\nabla p_{\mathrm{n}} - \varrho_{\mathrm{n}}\mathbf{g}\right)\right) - \nabla\cdot\left(\lambda_{\mathrm{pm}}\nabla T\right) = q^{\mathrm{h}}. \quad [2]$$

These equations are closed via

$$S_w + S_n = 1 \quad [3]$$

and the relation for the capillary pressure

$$p_c = p_n - p_w. \quad [4]$$

We use the model of Brooks and Corey (1964) for the relative permeabilities $k_{r\alpha}$ and the capillary pressure p_c.

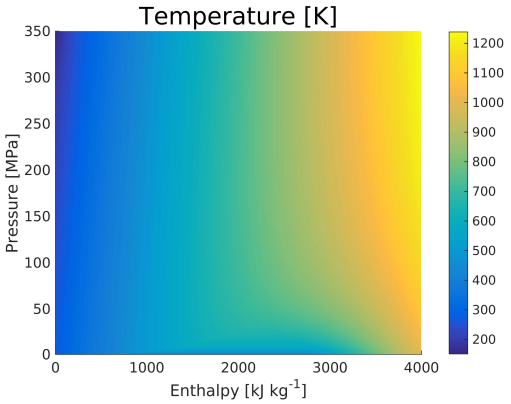

Figure 1: Variation of water temperature with pressure and enthalpy.

We consider water pressure p_w and enthalpy h as primary variables. Thus, saturations S_α and temperature T are only derived variables. Temperature can be calculated dependent on pressure and enthalpy. For this we use the IAPWS-95 relations of Wagner and Pruß (2002). Figure 1 shows the temperature dependent on pressure and enthalpy.

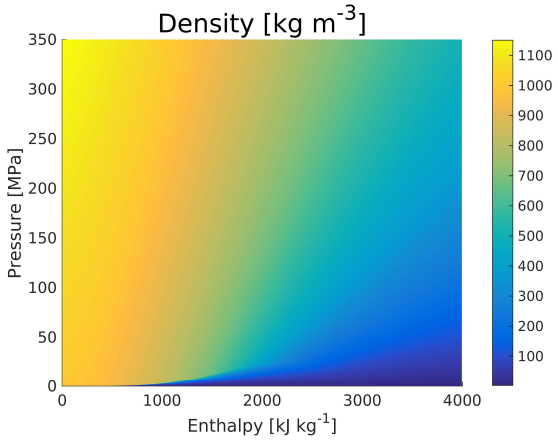

Figure 2: Variation of water density with pressure and enthalpy.

In single-phase regions, enthalpy is an unknown we solve for, $h_w = h$ or $h_n = h$. In two-phase regions, h_w and h_n are the saturated enthalpies, which also can be calculated after IAPWS-95 depending only on pressure. But in the two-phase case we still need to calculate the saturations. Here the following relation holds:

$$h = \frac{S_w\rho_w h_w + S_n\rho_n h_n}{\rho_w S_w + \rho_n S_n}. \quad [5]$$

Rearranging and using [3] we end up with

$$S_w = \frac{h\rho_n - h_n\rho_n}{h_w\rho_w - h_n\rho_n + h(\rho_n - \rho_w)}. \quad [6]$$

The remaining derived variables, such as density ρ_α, dynamic viscosity μ_α, internal energy u_α, all depend on pressure and enthalpy and are also calculated after IAPWS-95. As an example, Figure 2 shows the variation of density with pressure and enthalpy. The rock properties porosity ϕ, permeability $\boldsymbol{K}$, rock density ρ_s and heat capacity c_s vary only with position. The thermal conductivity of the water/steam filled porous medium is calculated as a geometric mean:

$$\lambda_{pm} = \lambda_s^{(1-\phi)}(\lambda_w S_w + \lambda_n S_n)^{\phi}. \quad [7]$$

3. Numerical Model

We use the implicit Euler method for the time discretization. This method is unconditionally stable and allows the use of large time-steps. A two-point flux approximation method is used for the space discretization. The domain is divided in quadrilaterals in two dimensions or cuboids in three dimensions. Let

us assume that we have two adjacent cells i and j. Then the discretized equations read

$$\sum_{\alpha} \phi \frac{(\rho_\alpha S_\alpha)_i^{n+1} - (\rho_\alpha S_\alpha)_i^n}{\Delta t} V_i + \sum_{\alpha} \sum_{j} \left(\rho_\alpha \frac{k_{r\alpha}}{\mu_\alpha} K\right)_{ij}^{n+1} \left(\frac{p_{w,j} - p_{w,i}}{d_i + d_j} - \rho_{ij} g_{ij}\right)^{n+1} A_{ij} - \sum_{\alpha} q_{\alpha,i}^{n+1} V_i = 0.$$

Here, A_{ij} denotes the area between cell i and j; V_i is the volume of cell i; d_i is the distance to the interface separating cells i and j with area A_{ij}; n and $n+1$ are time indices indicating the solution at step n and $n+1$.

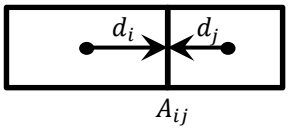

Figure 3: Two-point flux approximation for two neighboring grid cells i and j, with distances d_i and d_j to the interface separating the two control volumes with interface area A_{ij}.

The discretization of the energy equation is analogous. We use an upwinding strategy for $\left(\rho_\alpha \frac{k_{r\alpha}}{\mu_\alpha}\right)_{ij}$, harmonic averaging for K_{ij} and arithmetic averaging for the density in the gravity term. In the energy equation, enthalpies h are also upwinded.

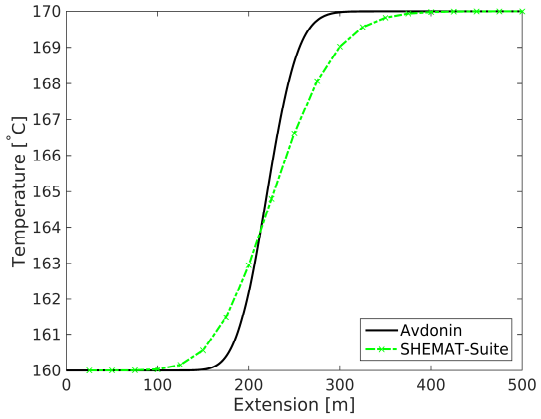

Figure 4: Avdonin solution vs. numerical solution from SHEMAT-Suite after 10^9 seconds.

After discretizing in space and time we end up with nonlinear algebraic systems. These are linearized with Newton's method. The derivatives of the Jacobian are automatically calculated via automatic differentiation (AD), a source code transformation which yields exact derivatives up to machine precision (Griewank and Walter, 2008; Rall, 1981). Finally, the linear systems are solved with PETSc, the portable extensible toolkit for scientific computing (Balay et al., 1997, 2014), providing a front-end to many different solvers and preconditioners. Next to the standard choice of BiCGStab (van der Vorst, 1992) with incomplete LU preconditioning, we can also use advanced solvers like algebraic multigrid methods (AMG), e.g., from the HYPRE (LLNL, 2016) package. For small systems a sparse direct method, MUMPS (Amestoy et. al. 2001, 2006), can be used for comparison.

4. VERIFICATION EXAMPLES

In this section we compare our numerical solution with available (semi-)analytical and numerical solutions. The test examples used are those of the 1980 Stanford code comparison study (SGP, 1980)

4.1 Avdonin solution - Injection

In this one-dimensional radial test problem water at 160 °C is injected into a geothermal reservoir with a temperature of 170 °C. At the left boundary, Neumann flow conditions with a flowrate of 10 kg s^{-1} are prescribed for mass, and temperature is fixed at 160 °C. At the right boundary pressure is fixed at 5 MPa and temperature at 170 °C. Avdonin (1964) gives a semi-analytical solution in integral form in terms of the Gamma function Γ and the complementary error function erfc. Properties for the model are shown in Table 1.

Table 1: Constant rock properties for the Avdonin solution.

Property	Letter	Unit	Value
Permeability	K	m^2	10^{-12}
Rock density	ρ_s	$kg\,m^{-3}$	2500
Rock specific heat capacity	c_s	$J\,kg^{-1}\,K^{-1}$	1000
Thermal conductivity	λ_{pm}	$W\,m^{-1}\,K^{-1}$	2
Porosity	ϕ	-	0.2

The reservoir is 100 m thick and the simulation domain extends over 1000 m, discretized into 40 equally spaced grid blocks. Figure 4 compares the numerical and the Avdonin solution for temperature, plotted over distance from the well after 10^9 seconds.

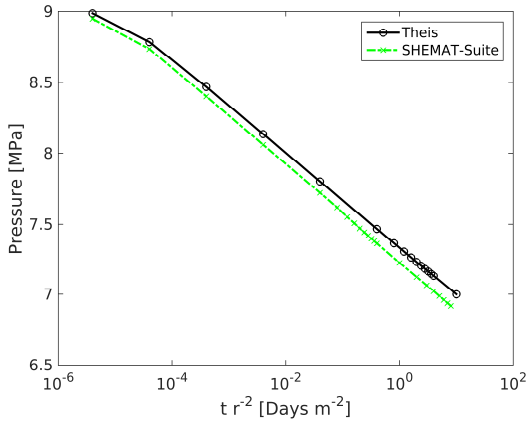

Figure 5: Theis solution vs. numerical solution from SHEMAT-Suite after 10^9 seconds.

4.2 Theis solution - Drainage

In this test example we compare the analytical Theis solution (Theis, 1935) for constant discharge with our one-dimensional radial numerical solution. Initially the reservoir is at 9 MPa and 260 °C. Thus, the fluid is

a single-phase liquid. The reservoir is 100 m thick. The grid spacing is chosen such that the discretization error is reduced. Cell centers are located at radii $r_n = 0.5 \cdot 2^{\frac{n-1}{2}}$ for $n = 1, \ldots, 26$. The total simulation time is one day. Figure 5 shows numerical and Theis solution as function of $t\,r^{-2}$ at a distance of 0.5 m from the injection well. Time is on a logarithmic scale.

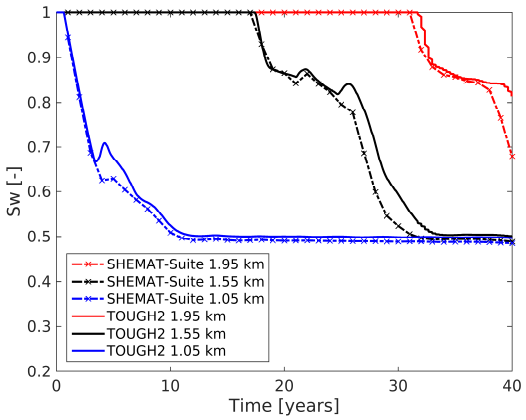

Figure 6: Water saturation over time for cells at the interface (1.05 km), in the middle of the lower layer (1.55 km) and at the bottom (1.95 km).

4.3 Expanding two-phase system with drainage

In this example the reservoir consists of two 1 km thick layers. The reservoir is pumped at the bottom at a rate of 100 kg s^{-1} km^{-2}. Initially the reservoir is in liquid state. A steam region will form near the top of the bottom layer. The space discretization is chosen as 20 blocks, each extending 100 m in z-direction. Initial temperature varies linearly from 10 °C at the surface to 290 °C at a depth of 1 km, and from 290 °C to 310 °C at 2 km depth. Rock properties are shown in Table 2. For the Brooks and Corey curves, we use a pore size distribution index of 2, a residual water saturation of $S_{wr} = 0.3$ and a residual gas saturation of $S_{nr} = 0.05$.

Table 2: Constant rock properties for two-phase example.

Property	Top layer	Bottom Layer	Unit
Permeability	$5 \cdot 10^{-15}$	10^{-13}	m^2
Rock density	2500	2500	$kg\,m^{-3}$
Rock specific heat capacity	1000	1000	$J\,kg^{-1}\,K^{-1}$
Rock thermal conductivity	1	1	$W\,m^{-1}\,K^{-1}$
Porosity	0.15	0.25	-

Figure 6 and 7 show the numerical solution obtained with SHEMAT-Suite vs. the numerical solution from TOUGH2 (Pruess et al., 1999).

5. Tuscan geothermal reservoir

The geological reservoir model comprising rock properties for the different layers is taken from Niederau et al. (2016). In this study we sample the available detailed geological model at much coarser spatial resolution yielding a model with only 48 000 cells. Naturally, this results in a poor resolution of the different geological units, but allows adapting the model rapidly and generating numerical solutions almost interactively. The most important geological structure in the model is the K horizon, which is assumed to be isothermal at a temperature of 450 °C (Liotta and Ranalli, 1999; Batini et al., 2003). The position of this isotherm, next to the assumed boundary conditions, is the main driving factor for the temperature distribution in our model.

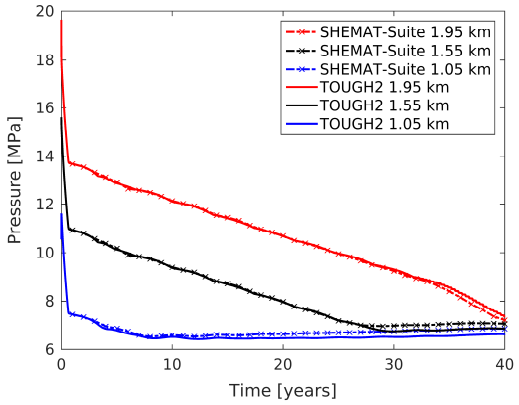

Figure 7: Pressure over time for cells at the interface (1.05 km), in the middle of the lower layer (1.55 km) and at the bottom (1.95 km).

5.1 Boundary and initial conditions

As initial conditions we assume a hydrostatic pressure distribution and a geothermal gradient of 30 K km^{-1} down to the K horizon. Thus, our domain is fully water saturated. The K horizon and all units below are assumed at 450 °C. The top boundary follows the earth's surface with a temperature of 11 °C and atmospheric pressure (0.101325 MPa). Lateral and bottom boundaries are closed for heat and mass flow.

5.2. PRELIMINARY RESULTS

The top of the K horizon extends upward to regions where the assumed temperature of 450 °C and the hydrostatic pressure gradient generate a steam cap at the beginning of the simulation (c.f. Figure 8).

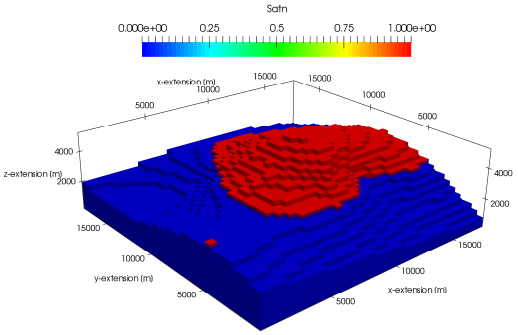

Figure 8: Formation of steam cap on top of the K horizon. Shown is gas saturation of K horizon cells.

Further on in time during our simulation, liquid flashes into steam in large parts of the domain. Figure 9 shows the steam saturation in the domain

after this huge flashing. This leads us to assuming that large parts of the domain are initially not in liquid but rather in steam state. This assumption seems to be confirmed by the few pressure data available from wells.

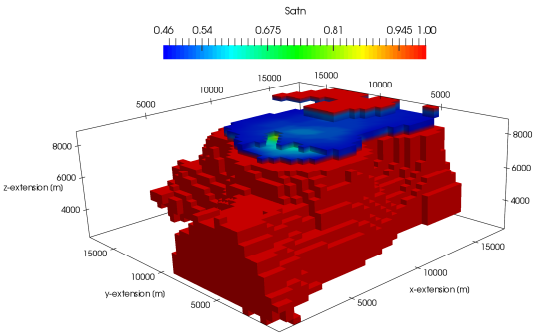

Figure 9: Huge flashing of most of the reservoir liquid into steam. Shown are cells with steam saturation of at least 0.46.

6. CONCLUSIONS

We implemented a pressure-enthalpy formulation into our in-house code SHEMAT-Suite allowing the simulation of two-phase water-steam reservoirs. The numerical solution of the governing equations has been verified by comparison with (semi-)analytical solutions, as well as numerical solutions from TOUGH2 in the case where no analytical solutions exist. We present first simulation results for a geothermal reservoir in Tuscany, Italy. These suggest that large parts of the domain are in steam rather than in liquid state.

Altogether, we are confident that our newly developed water-steam module for SHEMAT-Suite allows the simulation of geothermal reservoirs where transitioning from liquid to steam in a lot of cells occurs.

In the future we will conduct simulations for the Tuscan geothermal reservoir where we will assume a gas-static instead of a hydrostatic pressure gradient and calibrate our numerical model with temperature and pressure data available from boreholes in the region.

Acknowledgements

We thank ENEL Green Power for the opportunity to work with their data, as well as their open-minded discussion. We further thank Giordano Montegrossi for interesting modelling discussions, Zhi Yang Wong for helpful discussions regarding the verification examples and the PETSc developers, especially Barry Smith, Matthew Knepley and Jed Brown, for creating an extra-ordinary piece of software and their always prompt and helpful responses on the PETSc mailing list. Special thanks go to Anozie Ebigbo who always has an open ear for multi-phase flow questions.

This project is part of the H2020 Project DESCRAMBLE, financed by the European Union under grant 640573.

REFERENCES

Amestoy, P. R., Duff, I. S., L'Excellent, J.-Y., & Koster, J., 2001. A fully asynchronous multifrontal solver using distributed dynamic scheduling, *SIAM Journal on Matrix Analysis and Applications*, 23(1), 15–41.

Amestoy, P. R., Guermouche, A., L'Excellent, J.-Y., & Pralet, S., 2006. Hybrid scheduling for the parallel solution of linear systems, *Parallel Computing*, 32(2), 136–156.

Avdonin, N.A.: Some formulas for calculating the temperature field of a stratum subject to thermal injection: *Neft'i Gaz*,-V. 3, p.37-41 (1964).

Balay, S., Gropp, W. D., McInnes, L. C., & Smith, B. F., 1997. Efficient management of parallelism in object oriented numerical software libraries, in E. Arge, A. M. Bruaset, & H. P. Langtangen (eds.), *Modern Software Tools in Scientific Computing*, pp. 163–202, Birkh¨auser Press.

Balay, S., Abhyankar, S., Adams, M. F., Brown, J., Brune, P., Buschelman, K., Eijkhout, V., Gropp,W. D., Kaushik, D., Knepley, M. G., McInnes, L. C., Rupp, K., Smith, B. F., & Zhang, H., 2014. PETSc Users Manual, *Tech. Rep. ANL-95/11 - Revision 3.5*, Argonne National Laboratory.

Batini, F., Brogi, A., Lazzarotto, A., Liotta, D., and Pandeli, E.: Geological features of Larderello-Travale and Mt. Amiata geothermal areas (southern Tuscany, Italy). *Episodes*, *26*(3), 239-244, (2003).

Brooks, R. J., and A. T. Corey (1964), *Hydraulic properties of porous media*, vol. 3, Colorado State University Hydrology Paper.

Faust, C. R. and Mercer, J. W. (1979). Geothermal reservoir simulation: 2. numerical solution techniques for liquid- and vapor-dominated hydrothermal systems. *Water Resources Research*, 15(1):31–46.

Griewank, A. and Walther, A. (2008), *Evaluating Derivatives: Principles and Techniques of Algorithmic Differentiation*, number 105 *in* 'Other Titles in Applied Mathematics', 2nd edn, SIAM, Philadelphia, PA.

Lawrence Livermore National Laboratory, 2016. hypre: High Performance Preconditioners, http://www.llnl.gov/CASC/hypre/.

Liotta, D., and Ranalli, G.: Correlation between seismic reflectivity and rheology in extended lithosphere: southern Tuscany, inner Northern Apennines, Italy. *Tectonophysics*, *315*(1), 109-122, (1999).

Niederau, J., Büsing, H., Clauser, C., Jusri, T., Dini, I. Bertani, R., Impact of an uncertain structural model on geothermal reservoir simulations, *European Geothermal Congress 2016 Extended Abstract*, 2016.

Pruess, K., Oldenburg, C. M., and Moridis, G. J.: TOUGH2 User's Guide Version 2 (1999).

Rall, L. (1981), *Automatic Differentiation: Techniques and Applications*, Vol. 120 of *Lecture Notes in Computer Science*, Springer, Berlin.

Stanford Geothermal Program (SGP): *Proceedings of the Special panel on Geothermal Model Study, Report SGP-TR-42*, Stanford University, Stanford, CA (1980).

Theis, C V., 1935. The relation between the lowering of the piezometric surface and the rate and duration of discharge of a well using ground-water storage, *Trans. Am. Geophys. Union* 16, 519–524.

van der Vorst, H. A., 1992. Bi-CGSTAB: A fast and smoothly converging variant of Bi-CG for the solution of nonsymmetric linear systems, *SIAM Journal on Scientific and Statistical Computing*, 13(2), 631–644.

Wagner, W. and Pruß, A., *Journal of Physical and Chemical Reference Data*, 31, 387-535 (2002), DOI: http://dx.doi.org/10.1063/1.1461829